

Stochastic Inflation in Numerical Relativity

Yoann L. Launay,^{1,*} Gerasimos I. Rigopoulos,^{2,†} and E. Paul S. Shellard^{1,‡}

¹*Centre for Theoretical Cosmology, Department of Applied Mathematics and Theoretical Physics, University of Cambridge, Wilberforce Road, Cambridge CB3 0WA, United Kingdom*

²*School of Mathematics, Statistics and Physics, Newcastle University, Newcastle upon Tyne, NE1 7RU, United Kingdom*

A set of 3+1 equations for stochastic inflation incorporating all metric and scalar matter degrees of freedom, first presented in previous work [1], are re-derived in a gauge invariant manner. We then present numerical implementations of these stochastic equations, cast in the BSSN formulation of Numerical Relativity, demonstrating their efficacy in both a slow-roll and an ultra slow-roll scenario. We find the evolution is correctly reproduced for all the dynamical variables, and the energy and momentum constraints are well-satisfied. This demonstrates that the stochastic equations are theoretically and numerically robust and ready to be applied to a wider inflationary landscape. Our simulations result in real space realizations of the fully non-linear stochastic dynamics with gradient information retained. As a generalisation of standard stochastic inflation, inflationary numerical relativity and lattice cosmology, this work opens up the possibility for reliable predictions of non-perturbative phenomena and provides precise initial conditions for subsequent cosmological eras.

I. INTRODUCTION

Despite extensive theoretical advances, inflation remains relatively poorly constrained observationally. Cosmic microwave background (CMB) or large-scale structure (LSS) data for instance [2–4], is still too limited to probe inflationary interactions, the imprints of which lie in the so-called 3-point statistics. However, while ongoing experiments promise enriched data in the coming years, in particular on non-linear and potentially non-perturbative scales, substantial challenges remain when modeling connections from high-energy theories to data, and vice-versa. In fact, many scenarios of inflation remain untestable because current computational methods, whether theoretical or numerical, rely on numerous assumptions. For instance, quantum field theory on curved spacetimes [5–9] is usually limited to tree-level computations and thus truncated and perturbative non-linearity. On the other hand, historical approaches enabling non-perturbative and non-linear studies—which include stochastic inflation, stochastic and standard $\Delta\mathcal{N}$ formalisms, Hamilton-Jacobi approaches, lattice cosmology, and numerical relativity for inhomogeneous inflation [10–17]—do not fully complement QFT as they rely on gradient expansions, or approximate relativistic and quantum-to-classical effects. Beyond standard types of inflation, the landscape of testable scenarios is thus limited to those where strong leading-order approximations are valid.

With the expected arrival of smaller scales probes, Stochastic Inflation has become a popular non-perturbative method for studying the non-linear semi-classical evolution of long-wavelength inhomogeneities

during inflation, while still accounting for quantum diffusion. Its standard formulation relies on the separate universe approximation (SUA) or *Oth*-order gradient expansion, formulated in a specific gauge choice with the scalar field as the fluctuating dynamical variable and relies on the so-called stochastic $\Delta\mathcal{N}$ formalism to translate field fluctuations into statistics for the curvature perturbation [10, 18–25]. In our recent work [1], we showcased the theoretical generalisation of this approach by deriving the stochastic equations of full General Relativity for inflation, thus bypassing recent efforts to fix gradient expansions and gauge artifacts [26–28].

In this work we re-derive these equations without picking any gauge unlike the original derivations in ref. [1], which involved specific gauge families. These stochastic equations include all scalar and tensor degrees of freedom, metric and field alike, and are valid for any choice of time-slicing and threading of the spacetime. The derivation involves coarse-graining hypersurfaces by expressing them in terms of the coarse-grained curvature perturbation on comoving hypersurfaces \mathcal{R} . We then present a Numerical Relativity scheme where the stochastic inflation equations are solved for scalar sources in the synchronous gauge for two test scenarios: a slow roll potential and a potential with an inflection point with a transition to ultra slow-roll. This is distinct from a previous investigation of these scenarios with full GR evolution, where all perturbations are part of the initial conditions [29] (see also [30] for tensor modes).

We present the ADM stochastic equations and outline their derivation in Section II. Section III introduces the numerical implementation, and validates on the two aforementioned applications. We conclude in Section IV and leave in the Appendices the derivation of scalar gauge invariants in terms of \mathcal{R} (A), the full set of stochastic BSSN equations (B), details of the discrete schemes (C and D), and a first look at anisotropic DOFs (E).

* yoann.launay@outlook.com

† gerasimos.rigopoulos@ncl.ac.uk

‡ eps1@cam.ac.uk

II. STOCHASTIC GENERAL RELATIVITY

The stochastic equations of this section (16), (20), (21) and (24), (25) were first derived in ref. [1], where the source terms were obtained for diverse gauge families and coincided for all of them, leading us to conjecture gauge independence. In this section we provide a rigorous proof that these equations are indeed valid in all gauges.

A. Coarse-graining using \mathcal{R}

The derivation of the stochastic equations starts by considering a perturbed inflationary spacetime with a metric

$$ds^2 = -\alpha_b^2(1 + 2\Psi)dt^2 + 2a^2 B_{,i} dt dx^i + a^2 [(1 - 2\Phi)\delta_{ij} + 2E_{,ij}] dx^i dx^j, \quad (1)$$

where the four functions Φ, Ψ, B and E define the metric's scalar perturbations, with α_b and a the background lapse and scale factor. The scalar field driving the expansion is also perturbed as $\phi = \phi_b + \delta\phi$. The perturbations can be combined in the well-known linear gauge invariant quantities

$$\left\{ \begin{array}{l} \Phi + H\chi \quad \equiv \Phi_B, \\ \Psi - \dot{\chi} \quad \equiv \Psi_B, \\ \delta\phi - \dot{\phi}_b \chi \quad \equiv \delta\phi_{gi}, \\ -\Phi + \frac{\delta\rho}{3(\rho_b + P_b)} \equiv \zeta_{gi}, \\ \Phi + \frac{H}{\dot{\phi}_b} \delta\phi \quad \equiv \mathcal{R}, \end{array} \right. \quad (2)$$

where $\delta\rho = \alpha_b^{-2} \dot{\phi}_b \delta\dot{\phi} + V'|_b \delta\phi - \alpha_b^{-2} \dot{\phi}_b^2 \Psi$ is the scalar field energy density perturbation and $\chi \equiv -\alpha_b^{-1} a^2 (B - \dot{E})$. There are therefore five scalar perturbation variables which can be expressed in terms of the five gauge invariant variables.

We will take \mathcal{R} to be the fundamental dynamical variable of perturbations although others could be used. As shown in Appendix A and without relying on any further assumptions, the constraints equations can be used to obtain all other gauge-invariant variables in terms of \mathcal{R} and its derivatives in Fourier space [1]

$$\left\{ \begin{array}{l} \Phi_B = -\varepsilon_1 H a^2 k^{-2} \dot{\mathcal{R}}, \\ \Psi_B = \varepsilon_1 \mathcal{R} + \varepsilon_1 a^2 k^{-2} [\ddot{\mathcal{R}} + H(2 - \varepsilon_2)\dot{\mathcal{R}}], \\ \delta\phi_{gi} = \sqrt{2\varepsilon_1} M_{\text{Pl}} [\mathcal{R} + \varepsilon_1 a^2 H k^{-2} \dot{\mathcal{R}}], \\ \zeta_{gi} = -\mathcal{R} + \frac{1}{3} H^{-1} \dot{\mathcal{R}}, \end{array} \right. \quad (3)$$

where the slow-roll parameters are $\varepsilon_{i+1} \equiv -H^{-1} d_t \ln \varepsilon_i$, $\varepsilon_0 \equiv H$, in particular $\dot{\phi}_b^2 = 2\varepsilon_1 H^2 M_{\text{Pl}}^2$.

The first step in obtaining our stochastic equations is to now *coarse grain the fundamental variable* \mathcal{R}

$$\mathcal{R}_k \longrightarrow \mathcal{R}_k^> = W_k \mathcal{R}_k, \quad (4)$$

where W_k is a window function chosen to have support on long wavelengths: $W_0 = 1$ and $\lim_{k \rightarrow \infty} W_k = 0$, with

a relatively steep drop around a value $k = \sigma a H$ where σ a parameter determining the coarse-graining scale in terms of the Hubble radius $R_H = (aH)^{-1}$. The step function $W_k = \Theta(\sigma a H - k)$ is a common choice but smoother functions can also be envisaged - see (27) for the smooth window used here.

From now on coarse grained time derivatives are to be understood as $\dot{f}^> \equiv d(Wf)/dt$ in any linearized perturbation variable f . From the Sasaki-Mukhanov equation

$$\ddot{\mathcal{R}}_k + H(3 - \varepsilon_2)\dot{\mathcal{R}}_k + \frac{k^2}{a^2} \mathcal{R}_k = 0, \quad (5)$$

we then find that the coarse grained variable $\mathcal{R}_k^>$ obeys

$$\ddot{\mathcal{R}}_k^> + H(3 - \varepsilon_2)\dot{\mathcal{R}}_k^> + \frac{k^2}{a^2} \mathcal{R}_k^> = \mathcal{S}_{\mathcal{R}}, \quad (6)$$

where the spectral source term appearing on the r.h.s. is

$$\mathcal{S}_{\mathcal{R}} \equiv \mathcal{R}_k \ddot{W}_k + [2\dot{\mathcal{R}}_k + (3 - \varepsilon_2)H\mathcal{R}_k] \dot{W}_k. \quad (7)$$

Note that $\mathcal{S}_{\mathcal{R}}$ vanishes when the window is constant and therefore its existence is solely attributed to the time-dependent UV-IR split or to initial conditions.

The second step is to replace $\mathcal{R} \rightarrow \mathcal{R}^>$ on the r.h.s. of (3) and use (6) to replace the second time derivative term. This *defines* our coarse grained linear gauge invariant variables as

$$\left\{ \begin{array}{l} \Phi_B^> = -\varepsilon_1 a^2 k^{-2} H \dot{\mathcal{R}}^>, \\ \Psi_B^> = -\varepsilon_1 a^2 k^{-2} (H \dot{\mathcal{R}}^> - \mathcal{S}_{\mathcal{R}}), \\ \delta\phi_{gi}^> = \sqrt{2\varepsilon_1} M_{\text{Pl}} [\mathcal{R}^> + \varepsilon_1 a^2 H k^{-2} \dot{\mathcal{R}}^>], \\ \zeta_{gi}^> = -\mathcal{R}^> + \frac{1}{3} H^{-1} \dot{\mathcal{R}}^>. \end{array} \right. \quad (8)$$

These relations are then inserted into the r.h.s. of (2) to define the coarse grained scalar perturbation variables $\Phi^>, \Psi^>, \chi^>$ and $\delta\phi^>$ in terms of $\mathcal{R}^>$ and $\dot{\mathcal{R}}^>$, also explicitly containing $\mathcal{S}_{\mathcal{R}}$

$$\left\{ \begin{array}{l} \Phi^> + H\chi^> = -\varepsilon_1 a^2 k^{-2} H \dot{\mathcal{R}}^>, \\ \Psi^> - \dot{\chi}^> = -\varepsilon_1 a^2 k^{-2} (H \dot{\mathcal{R}}^> - \mathcal{S}_{\mathcal{R}}), \\ \delta\phi^> - \dot{\phi}_b \chi^> = \sqrt{2\varepsilon_1} M_{\text{Pl}} [\mathcal{R}^> + \varepsilon_1 a^2 H k^{-2} \dot{\mathcal{R}}^>], \\ -\Phi^> + \frac{\delta\rho^>}{3(\rho_b + P_b)} = -\mathcal{R}^> + \frac{1}{3} H^{-1} \dot{\mathcal{R}}^>, \\ \Phi^> + \frac{H}{\dot{\phi}_b} \delta\phi^> = \mathcal{R}^>. \end{array} \right. \quad (9)$$

Each of the coarse-grained scalar perturbation variables of the l.h.s. can now be solved for and, as a final step, inserted into the linearized version of Einstein's equations in their ADM form. After further use of (6) and resulting cancellations of terms, the only terms that survive involve $\mathcal{S}_{\mathcal{R}}$, becoming the sources in the stochastic equations. We illustrate this procedure in the following subsection by explicitly performing it for the field equation.

B. Gauge invariant coarse-graining: field equation

As an explicit example of the procedure described in the previous subsection, we now demonstrate the coarse-

graining of the ADM inflaton equation

$$\frac{1}{\alpha} \left(\dot{\Pi} + \beta^i \Pi_{|i} \right) - K\Pi - \frac{\alpha^{|i}}{\alpha} \phi_{|i} - \phi_{|i}^i + \frac{dV}{d\phi} = 0, \quad (10)$$

where $\Pi = \alpha^{-1}(\dot{\phi} + \beta^i \partial_i \phi)$ and as usual, $K = -3H$. Before coarse-graining, the corresponding linear field equation in Fourier space is

$$\begin{aligned} \delta\ddot{\phi} + 3H\delta\dot{\phi} + \frac{k^2}{a^2}\delta\phi - \dot{\phi}_b \left(3\dot{\Phi} + \dot{\Psi} + \frac{k^2}{a^2}\chi \right) \\ + \frac{d^2V}{d\phi^2}(\phi_b)\delta\phi + 2\Psi \frac{dV}{d\phi}(\phi_b) = 0 \end{aligned} \quad (11)$$

where α_b was set to 1 without loss of generality. We want to calculate the spectrum of the *r.h.s.* of the same equation but for the IR field perturbations ($\delta\phi^>, \Phi^>, \Psi^>, \chi^>$).

Using eq. (9) and *without picking a gauge*, it is possible to express all these linear degrees of freedom as functionals of $\mathcal{R}^>$ and another scalar of our choice. In the case of the field equation, we choose this scalar to be the inflaton's perturbation $\delta\phi^>$. Eq. (9) can then be rearranged

$$\begin{cases} \Phi^> = \mathcal{R}^> - \dot{\phi}_b^{-1} H \delta\phi^> \\ \chi^> = \dot{\phi}_b^{-1} \delta\phi^> - H^{-1} \mathcal{R}^> - \varepsilon_1 a^2 k^{-2} \dot{\mathcal{R}}^>, \\ \Psi^> = \dot{\chi}^> - \varepsilon_1 a^2 k^{-2} (H \dot{\mathcal{R}}^> - \mathcal{S}_{\mathcal{R}}). \end{cases} \quad (12)$$

By making further use of eq. (6), the time differentiations needed in the coarse-graining of (11) can be expressed as

$$\begin{cases} \dot{\Psi}^> = H(\varepsilon_1 + \frac{1}{2}\varepsilon_2)\dot{\phi}_b^{-1}\delta\phi^> + \dot{\phi}_b^{-1}\delta\dot{\phi}^> - H^{-1}\dot{\mathcal{R}}^> \\ \dot{\Phi}^> = \dot{\mathcal{R}}^> - H\dot{\phi}_b^{-1}\delta\phi^> - \frac{1}{2}\varepsilon_2 H^2 \dot{\phi}_b^{-1}\delta\phi^> \\ \dot{\Psi}^> = \dot{\phi}_b^{-1}\delta\ddot{\phi}^> + (2\varepsilon_1 + \varepsilon_2)H\dot{\phi}_b^{-1}\delta\dot{\phi}^> \\ \quad + \frac{1}{4}\varepsilon_2(-2\varepsilon_1 + \varepsilon_2 - 2\varepsilon_3)H^2\dot{\phi}_b^{-1}\delta\phi^> \\ \quad + a^2 H^{-1} k^2 \mathcal{R} + (3 - \varepsilon_1 - \varepsilon_2)\dot{\mathcal{R}} \\ \quad - H^{-1}\mathcal{S}_{\mathcal{R}}. \end{cases} \quad (13)$$

Replacing these, together with the previous eq. (12) and

$$\begin{cases} \frac{dV}{d\phi}(\phi_b) = (-3 + \varepsilon_1 + \varepsilon_2/2)H\dot{\phi}_b^{-1}, \\ \frac{d^2V}{d\phi^2}(\phi_b) = -\frac{1}{4}[8\varepsilon_1^2 + 2\varepsilon_1(-12 + 5\varepsilon_2) \\ \quad + \varepsilon_2(-6 + \varepsilon_2 + 2\varepsilon_3)]H^2, \end{cases} \quad (14)$$

into the the l.h.s. of (11), all terms perfectly cancel apart from the Mukhanov-Sasaki-Starobinsky term $\mathcal{S}_{\mathcal{R}}$ which survives as a source term. One therefore sees that the IR version of eq. (11) is

$$\begin{aligned} \delta\ddot{\phi}^> + 3H\delta\dot{\phi}^> + \frac{k^2}{a^2}\delta\phi^> - \dot{\phi}_b \left(3\dot{\Phi}^> + \dot{\Psi}^> + \frac{k^2}{a^2}\chi^> \right) \\ + \frac{d^2V}{d\phi^2}(\phi_b)\delta\phi^> + 2\Psi^> \frac{dV}{d\phi}(\phi_b) = \dot{\phi}_b H^{-1} \mathcal{S}_{\mathcal{R}}, \end{aligned} \quad (15)$$

in agreement with the equation presented in previous work [1], but proven here for *all gauge choices*.

Similarly to standard derivations of stochastic inflation, the obtained r.h.s. is now assumed to provide the spectrum of the random variable making up the stochastic noise term for the full non-linear version of (11), giving the ADM inflaton equation

$$\frac{1}{\alpha} \left(\dot{\Pi} + \beta^i \Pi_{|i} \right) - K\Pi - \frac{\alpha^{|i}}{\alpha} \phi_{|i} - \phi_{|i}^i + \frac{dV}{d\phi}(\phi) = \mathcal{F}^{-1}\{\mathcal{S}_{\Pi}\}, \quad (16)$$

where $\mathcal{F}^{-1}\{\cdot\}$ is the inverse hermitian Fourier transform and where the stochastic field is

$$\mathcal{S}_{\Pi} = \sqrt{2\varepsilon_1} M_{\text{Pl}} \mathcal{S}_{\mathcal{R}} \alpha_{\vec{k}}, \quad (17)$$

the amplitude of which is controlled by the mode functions of the gauge invariant perturbation \mathcal{R} obeying the non-coarse-grained linear equation (5). The random field \mathcal{S} includes the gaussian random variables $\alpha_{\vec{k}}$ such that for all (\vec{k}, \vec{k}') in the same Fourier hemisphere

$$\begin{cases} \langle \alpha_{\vec{k}} \alpha_{\vec{k}'} \rangle_{\mathbb{P}} = 0, \\ \langle \alpha_{\vec{k}} \alpha_{\vec{k}'}^* \rangle_{\mathbb{P}} = \delta^{(3)}(\vec{k} - \vec{k}'). \end{cases} \quad (18)$$

To match the Gaussian spectrum of the quantum operators, one should take $\alpha_{\vec{k}} \sim \mathcal{CN}(0, 1)$, which is equivalent to $\text{Real}[\alpha_{\vec{k}}], \text{Im}[\alpha_{\vec{k}}] \sim \mathcal{N}(0, 1/2)$ independently or $|\alpha_{\vec{k}}| \sim \text{Rayleigh}(1/\sqrt{2})$ and $\text{Arg}[\alpha_{\vec{k}}] \sim \mathcal{U}(0, 2\pi)$. In the following, the stochastic IR **bold** notation of the LHS will be kept implicit for notational simplicity.

C. Full ADM Stochastic Inflation

The procedure of inserting the coarse grained perturbation variables in the l.h.s of the linearized versions of the dynamical equations, and thus obtaining the resulting source term, can also be performed for the other dynamical equations. In this section, we present the result of the application of this procedure to the remaining equations of the ADM formulation: a set of stochastic dynamical equations for the extrinsic curvature of the spatial slices that are valid for any choice of coordinates, while satisfying the usual Energy and Momentum constraints. By construction, standard linear perturbation theory is recovered for the coarse grained variables when this system is linearized. In particular, one can re-derive (6) by working backwards. Clearly, if no time dependent long-short split is performed $\dot{W}_k = 0$, all standard equations are recovered. However, equations (16) - (20) - (21) and (24) - (25) are non-linear and can capture any non-linear development once modes have crossed the horizon as set by W .

Using the ADM 3+1 foliation notations for the metric

$$ds^2 = -\alpha^2 dt^2 + \gamma_{ij} (dx^i - \beta^i dt) (dx^j - \beta^j dt), \quad (19)$$

the equations of the ADM formulation of General Relativity can be extended to a set of dynamical stochastic equations. In particular, the extrinsic curvature defined as $K_{ij} \equiv - (2\alpha)^{-1} (\gamma_{ij,0} + \beta_{ij} + \beta_{j|i})$ is found to obey

$$\begin{aligned} & \dot{K} + \beta^i K_{,i} + \alpha^{|i}{}_{|i} - \alpha ({}^3R + K^2) \\ & - M_{\text{Pl}}^{-2} \alpha \left(\frac{1}{2} S - \frac{3}{2} \rho \right) = \mathcal{F}^{-1} \{ \mathcal{S}_K \}, \end{aligned} \quad (20)$$

and

$$\begin{aligned} & \dot{\tilde{K}}_{ij} + 2\alpha \tilde{K}_{il} \tilde{K}^l{}_j + \beta^k \tilde{K}_{ij|k} - 2\beta_i{}^{|k} \tilde{K}_{jk} \\ & + \alpha^{|i}{}_{|j} - \frac{1}{3} \alpha^{|k}{}_{|k} \delta_{ij} - \alpha \left({}^3\tilde{R}_{ij} + \frac{1}{3} K \tilde{K}_{ij} \right) \\ & + M_{\text{Pl}}^{-2} \alpha \tilde{S}_{ij} = \mathcal{F}^{-1} \{ \mathcal{S}_{\tilde{K}_{ij}} \}, \end{aligned} \quad (21)$$

where we wrote $K_{ij} = \tilde{K}_{ij} + \frac{1}{3} \delta_{ij} K$, expressing it in terms of the traceless \tilde{K}_{ij} and trace K parts, and sourced by the stress tensor components $\rho = \alpha^2 T^{00}$, $\mathcal{J}_i = \alpha T^0{}_i$, $S_{ij} = T_{ij}$. A vertical bar denotes a covariant derivative associated with γ_{ij} . The source terms appearing on the r.h.s. of the above equations are

$$\mathcal{S}_K = -\varepsilon_1 \mathcal{S}_{\mathcal{R}} \alpha_{\vec{k}}, \quad (22)$$

$$\mathcal{S}_{\tilde{K}_{ij}} = a^2 \varepsilon_1 \left(\frac{1}{3} \delta_{ij} - k^{-2} k_i k_j \right) \mathcal{S}_{\mathcal{R}} \alpha_{\vec{k}}, \quad (23)$$

sharing the same random lattice draw as eq. (17). Note that a similar coarse-graining can be performed for the quantised graviton degrees of freedom to give an additional source in the \tilde{K}_{ij} evolution [1] but this work focuses on scalar input.

The dynamical equations are supplemented by the two ADM constraints

$$\mathcal{H} \equiv {}^3R + \frac{2}{3} K^2 - \tilde{K}_{ij} \tilde{K}^{ij} - 2M_{\text{Pl}}^{-2} \rho = 0, \quad (24)$$

$$\mathcal{M}_i \equiv \tilde{K}^j{}_{i|j} - \frac{2}{3} K_{|i} - M_{\text{Pl}}^{-2} \mathcal{J}_i = 0, \quad (25)$$

which *do not* receive any stochastic terms on the r.h.s. Indeed, inserting the coarse grained variables in the linearized l.h.s leads to complete cancellations and no source terms appear. This is an important property of the stochastic augmentation of the ADM system of equations: the dynamics can be seen as a continuous succession of "drift and kick" evolution steps or a "continuous readjustment of initial conditions" [12]. The l.h.s. of the ADM equations (16) - (20) - (21) preserves the constraints if initial conditions satisfy them. Indeed, satisfying the constraints is an important consideration in any scheme for setting initial conditions in Numerical Relativity. Since the stochastic source terms can be interpreted as modifying the "initial conditions" for each successive time step, their addition must not alter the ADM constraints. Our approach for defining these stochastic source terms satisfies the constraints at first order by construction.

Potential	Quadratic	Higgs inflection [34, 35]
Expression	$V[\phi] = \frac{1}{2} m^2 \phi^2$	$V[\phi] = \frac{\Lambda v^4 \phi^2 (3\phi^2 + 2\sqrt{2}\phi v + 6v^2)}{3(3\phi^2 + 2v^2)^2}$
Parameters	$\varepsilon_1 = 0.01$ $\varepsilon_2 = -0.02$ $H_0 = 10^{-5} M_{\text{Pl}}$ $m = m(\varepsilon_1, \varepsilon_2, H_0)$ $\phi_0 = \phi_0(\varepsilon_1, \varepsilon_2, H_0)$	$\Lambda = 1.86 \times 10^{-6}$ $v = 0.198 M_{\text{Pl}}$ $\phi_0 = -1.2 M_{\text{Pl}}$ $\varepsilon_1 = \varepsilon_1(\phi_0)$ $H_0 = H_0(\varepsilon_1, \phi_0)$
Simulation	$\mathcal{N}^\circ - \mathcal{N}_0 \sim 5$ $\mathcal{N}_f - \mathcal{N}^\circ \sim 8$	$\mathcal{N}^\circ - \mathcal{N}_0 \sim 3$ $\mathcal{N}_f - \mathcal{N}^\circ \sim 10$

TABLE I: Potentials used in this study and their parameters, including initial conditions, determined either by *potential-position* or H_0 fixing [29]. \mathcal{N}_0 , \mathcal{N}° , and \mathcal{N}_f are the Bunch-Davies initialisation time, the start of the NR simulation, and the final time in e-folds.

The stochastic equations derived here rely on linearized perturbations for determining the noise terms and this is an approximation that underlies practically all derivations of stochastic equations for inflation. However, the subsequent evolution of the long wavelength configuration is fully non-linear. Overall, this "linearized noise" approximation together with neglecting the quantum contributions to the interactions (expected to hold from horizon crossing [31]) and the stochastic backreaction of IR fields on the UV modes that determine the noise, are the only approximations left in the above equations.

We note here that a possible heuristic inclusion of the backreaction of the long wavelength inhomogeneous fields on the UV modes used to compute the noise, is the promotion of the background parameters in the equation determining the solution for the UV modes into functions of those spatially-dependent long wavelength fields [12, 22, 23, 32]. Following this general approach, in this work we include the possibility of such long-wavelength backreaction on short wavelength modes by including the evolution of the Mukhanov-Sasaki eq. (5) in real space

$$\begin{cases} \Pi_{\mathcal{R}} = \frac{\gamma}{\alpha} \left(\partial_0 \mathcal{R} + \beta^i \partial_i \mathcal{R} \right) \\ \partial_0 \Pi_{\mathcal{R}} - \alpha K \Pi_{\mathcal{R}} + \beta^i \partial_i \Pi_{\mathcal{R}} - \gamma \alpha \partial_i \partial^i \mathcal{R} = 0, \end{cases} \quad (26)$$

solved simultaneously with (16) - (20) - (21) and (24) - (25). Here, $\gamma \equiv z^2/a^2 = \dot{\phi}_b^2/H^2$ and $\mathcal{R}(t, \mathbf{x})$ is a real space variable whose Fourier transform at any time provides the modes for the computation of any stochastic r.h.s. \mathcal{S} term. The evolution in real space is the key for including stochastic backreaction by promoting all the background quantities in the equation's coefficients to their local values: $\gamma_b \rightarrow \gamma(t, x^i)$, $K_b \rightarrow K(t, x^i)$, $\alpha_b \rightarrow$

$\alpha(t, x^i)$.¹, making the input noise non-Gaussian.

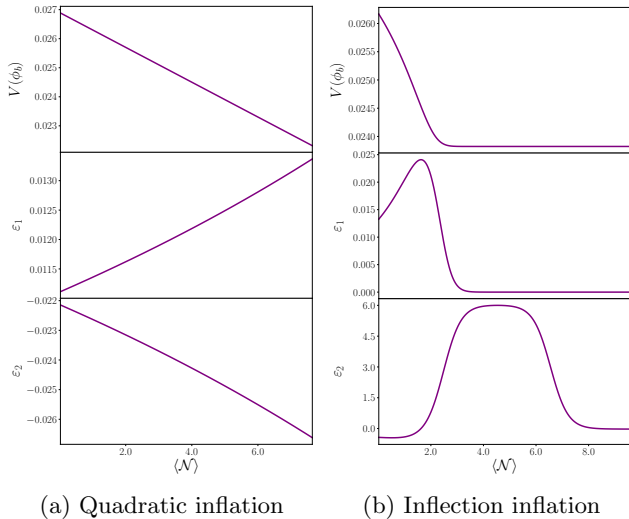


FIG. 1: Time background evolution of the potential value (top), first (middle) and second (bottom) slow-roll parameters for both our validation scenarios. Perfect agreement between Friedmann and NR evolutions. $M_{\text{Pl}} = 100$.

III. STOCHASTIC NUMERICAL RELATIVITY

A. Numerical Pipeline

Numerically solving eqns. (16), (20) and (21) from initial data, while satisfying (24) and (25), requires a well-posed reformulation leading to the BSSN equations and variables [36, 37] presented in Appendix B. These equations along with (26) for the noise amplitude, with or without long wavelength backreaction, are the main equations of our stochastic inflation formulation for numerical relativity (NR). To our knowledge, there is currently no other stochastic NR code whether it is for an inflating spacetime or not.

Before incorporating any stochasticity, multiple codes are available to solve the BSSN system. In this work, we chose to use the most recent GRTECLYN [38]². It inherits the AMREX software [41] within its core, which enables the efficient scalable use of GPU offloading and adaptive mesh refinement (AMR) to solve generic PDEs with finite volume methods. In this work, the numerical

¹ To our knowledge, such a scheme was first proposed but not numerically implemented in [12]. More recently, a similar construction for the mode equations was numerically implemented in [22, 23, 33].

² Note that an official public release is not yet available, but the software is open-access and reproduces the scalar sector of [29] against the well established GRCHOMBO [39, 40].

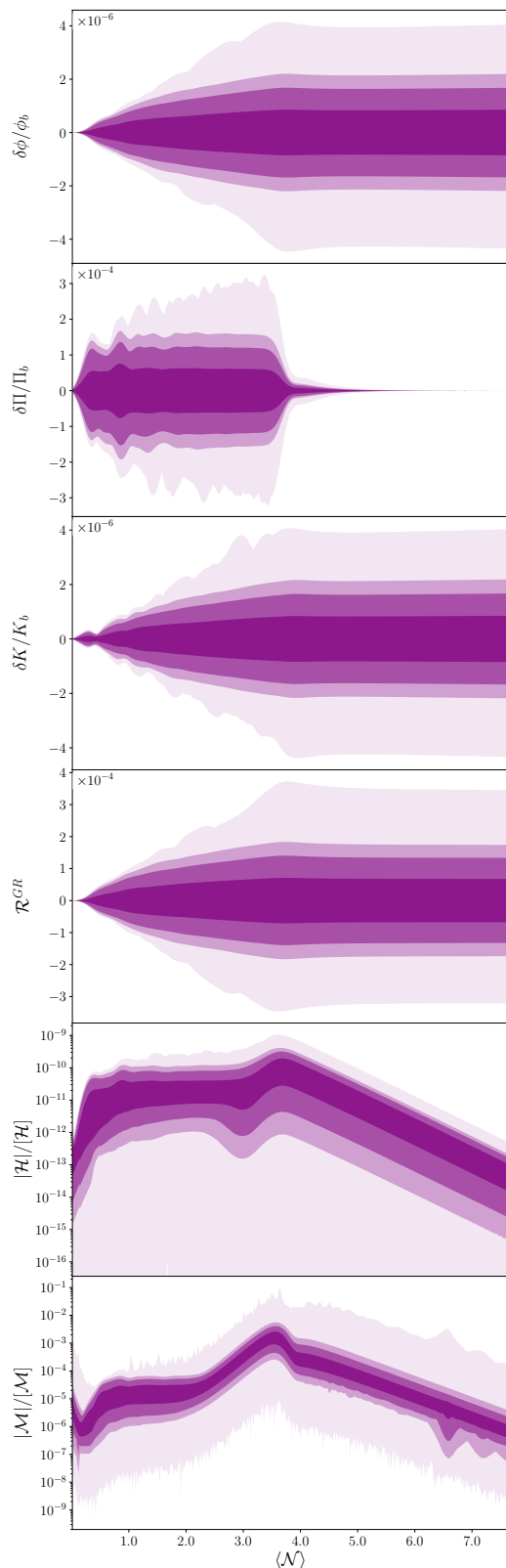


FIG. 2: Contrast of the inflaton (top), its momentum, the extrinsic curvature, the reconstructed \mathcal{R}^{NR} and the relative Hamiltonian and Momentum constraints (bottom) extracted from the NR simulation of quadratic inflation using 68, 95, 99 and 100 percentile contours (dense to light purple). $M_{\text{Pl}} = 100$.

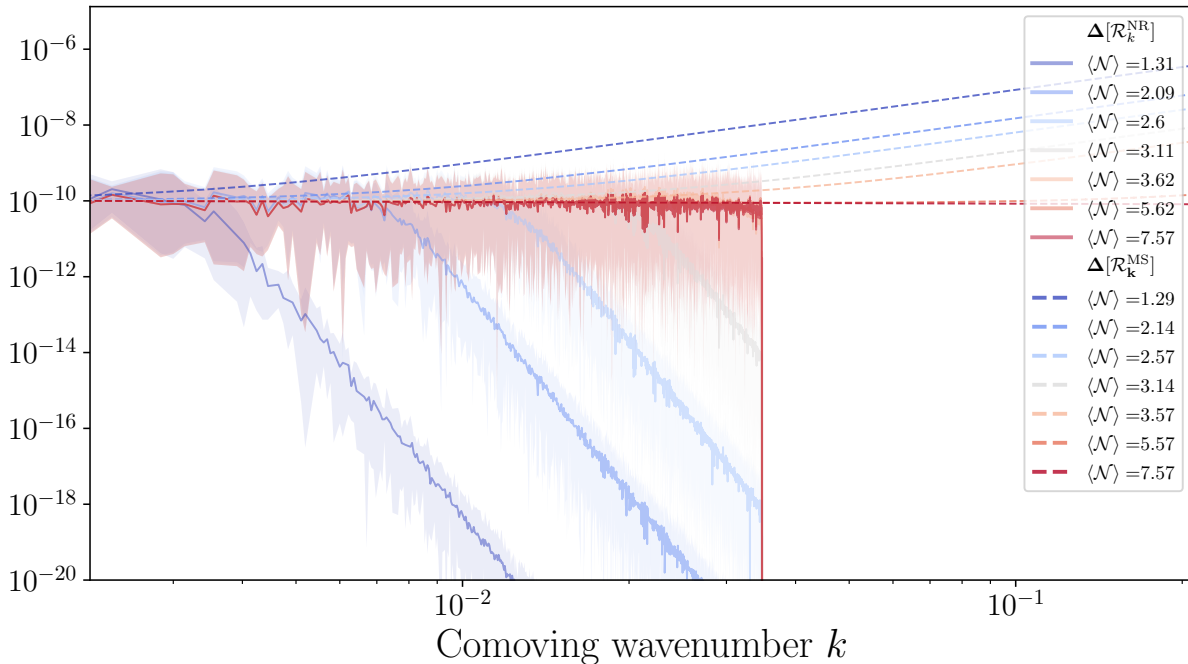


FIG. 3: Linear (dashed, \mathcal{R}^{MS}) and reconstructed (solid, \mathcal{R}^{NR}) binned dimensionless spectra ($\Delta[\cdot] = \frac{k^3}{2\pi^2} |\cdot|^2$) in the quadratic inflation case from initial (navy blue) to final (red) times. Contours account for the full range of points in each bin. Fourier bins are those of the lattice with more than 10 realisations. $M_{\text{Pl}} = 100$.

scheme of the time evolution is a 4th order Runge-Kutta (RK4).

With GRTECLYN as its core, ISTORIZ³ enables the specific study of inflation together with the stochastic sources derived above. In its current version, ISTORIZ sets NR parameters to fairly simple values. The AMR is switched off together with the damping of the constraints (CCZ4 [42, 43]), the gauge choice is that of geodesic slicing (cosmic time, $\alpha = 1$, $\beta^i = 0$), and we use periodic boundary conditions. Up to caveats of studying cosmological spacetimes in NR [44], these only constitute arbitrary choices to which the software is not limited. Given the spectral nature of our stochasticity, using AMREX-based software, such as GRTECLYN, has additional advantages because of the built-in off-loaded Fast Fourier Transform (FFT) capabilities. Key components of ISTORIZ are:

- i) Reading of inflationary background initial conditions (ϕ_b^\otimes , Π_b^\otimes , K_b^\otimes , X_b^\otimes) and spectral initial conditions for the curvature perturbation on comoving hypersurface (\mathcal{R}_k^\otimes and $\partial_t \mathcal{R}_k^\otimes$ for each k of the discrete Fourier lattice). In this work, these are all provided by the STOIIIC generator presented in [29], using *oscode* [45] to solve the Mukhanov-Sasaki equation from deep subHubble initialisation (time \mathcal{N}_0) to the

start of the simulation (time \mathcal{N}^\otimes) when the first mode enters the defined IR (σ -dependent).

- ii) Random draw of the real space Gaussian discrete fields $\mathcal{R}^\otimes(\mathbf{x})$ and $\partial_t \mathcal{R}^\otimes(\mathbf{x})$ from the input spectra (see methodology in [29] and [30]), and, in parallel to the BSSN evolution, evolution of the Mukhanov-Sasaki eq. (5) in real space in its well-posed formulation eq. (26). Stochastic backreaction can be switched on in this evolution, by promoting background quantities such as γ , K_b or X_b to their local spatial value.
- iii) At each time step, the discrete stochastic contribution is computed by i) Transforming $\mathcal{R}(t, \mathbf{x})$ and $\partial_t \mathcal{R}(t, \mathbf{x})$ to Fourier space, ii) Computing $\int_t^{t+\Delta t} \mathcal{S}_X(u, k) du$, $X = \{\Pi, K, A_{ij}\}$, iii) Transforming back to real space $\mathcal{F}^{-1}\{\cdot\}$, iv) Adding this stochastic noise to each r.h.s. of the discretised BSSN, to satisfy the constraints up to $\mathcal{O}(\text{noise}^2)$. See Section C for details on the stochastic scheme.

B. Design of the discrete stochastic spacetime

The choice of a geodesic gauge implies that our lattice is a comoving space one. In these coordinates, the Hubble radius $R_H = (aH)^{-1}$ shrinks so that big scales receive our stochastic fluctuations first, followed by smaller ones until reaching the lattice's smallest visible scale (dx).

³ Inflationary STOchastic Relativity Integrator for zeta.

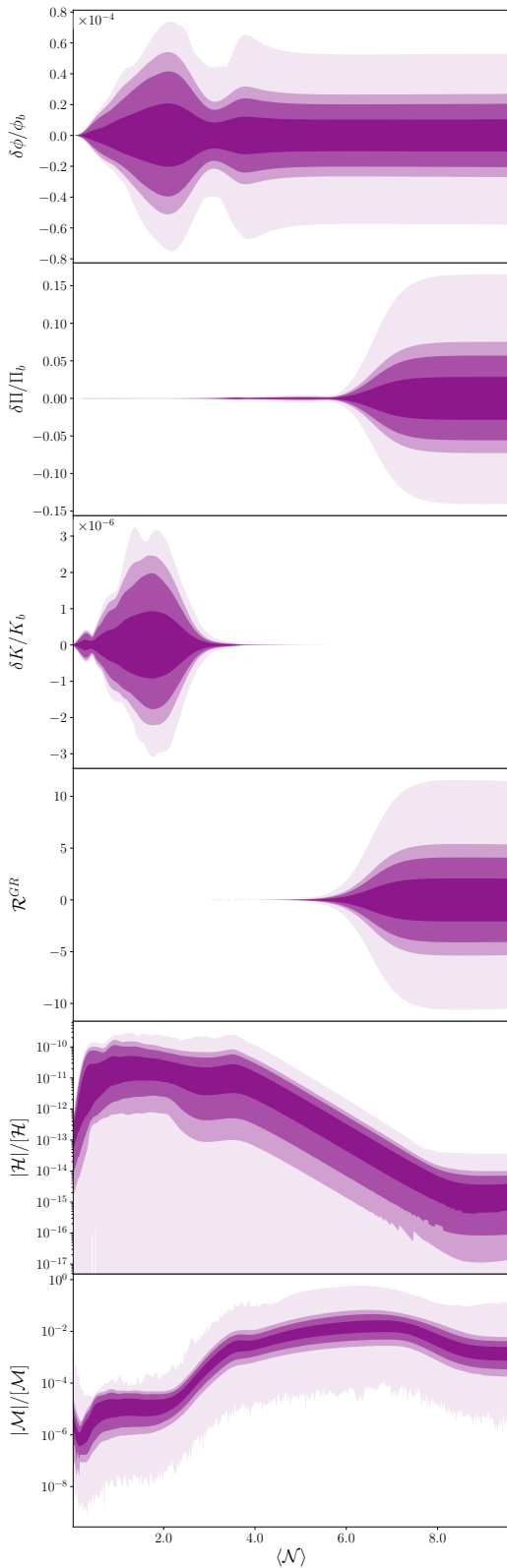


FIG. 4: Contrast of the inflaton (top), its momentum, the extrinsic curvature, the reconstructed \mathcal{R}^{NR} and the relative Hamiltonian and Momentum constraints (bottom) extracted from the NR simulation of inflection inflation using 68, 95, 99 and 100 percentile contours (dense to light purple). $M_{\text{Pl}} = 100$.

In this work, each mode k evolved by eq. (5) or (26) enters the GR evolution via the stochastic terms when $k_\sigma(t) \equiv \sigma R_H^{-1}(t)$ has increased up to k . This is practically the case when the window function is set to the rolling rectangle $\Theta[k_\sigma(t) - k]$. However, to demonstrate the generality of our framework and resolve all involved time derivatives of W , we pick a smoother window function with activation centered on the crossing

$$W_k(t) = \frac{1}{2} \left(1 + \tanh \left[s \log \left(\frac{k_\sigma(t)}{k} \right) \right] \right), \quad (27)$$

where $s = 5.0$ is an arbitrary sharpness parameter⁴. Thanks to a random draw performed in Fourier space and the Fourier transforms at every time step, we effectively input non-Markovian noise when such a non-sharp window function is used.

Let N now be the number of cells per spatial dimension of the simulation's cubic patch of universe and $L = Ndx$ the unitfull comoving size of the latter. Assuming real fields and the usual isotropy of the fluctuations, the range of Fourier modes which can be added is thus made of all norms k such that $k = dk\sqrt{a^2 + b^2 + c^2}$, where $(a, b, c) \in [[0, \lfloor N/2 \rfloor]]^3$ and $dk \equiv k_{\text{min}} = 2\pi L^{-1}$. In this setting, STOIC picks L so that the first mode enters when the simulation starts, which is $Lk_\sigma^\circledast = 2\pi$. Note, however, that our UV cutoff for the fluctuations is usually taken lower than the Nyquist one since gradients use $n = 4$ to 6 cells and need to be resolved for the satisfaction of the constraints, hence imposing $k_{\text{max}}^{\mathcal{R}} = Nk_\sigma^\circledast/n$ as the last mode to enter the GR simulation. In practice, we find that these high- k modes benefit from an even harder UV cutoff, which is why we cut with $n = 7$.⁵

Similarly, the design of the time dimension in the lattice or stepping is intrinsically linked to the amount of physical time we are interested in and to the available computational resources constraining the choice of N . This is explained in Appendix D.

C. Validation

In the following, we work with the scaling $a^\circledast = 1$, units such that $M_{\text{Pl}} = 100$ and lattices of size $N = 256$. The coarse-graining is fixed to $\sigma = 1$ for all scenarios. Back-reaction is switched on. Similarly to our previous work [29], we study both a vanilla example of inflation for the sake of diagnostics, and a more challenging example of

⁴ This should not have an impact on the result in the late-time limit, as long as a window follows requirements such as those defined in [46]. However, for a given discrete scheme, not all windows are suitable. In particular the sharpness should be appropriate for the time stepping and for keeping all terms within perturbation theory.

⁵ Note that Kreiss-Oliger dissipation is also available in GRTECLYN to damp out high frequency modes, but not deployed here.

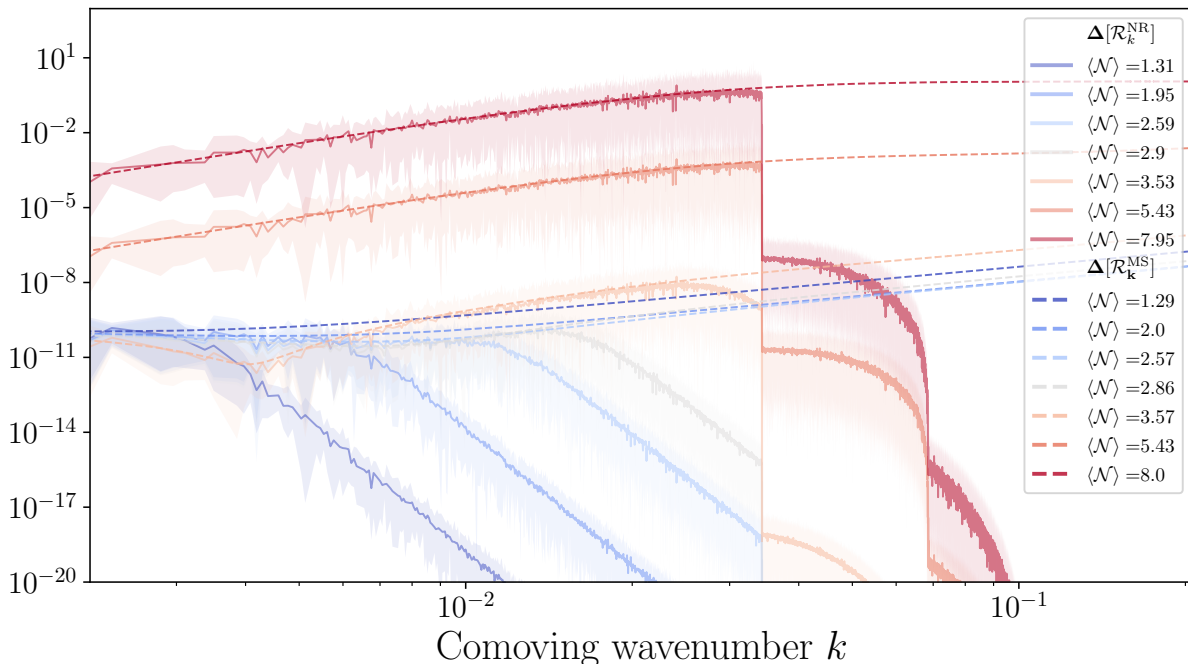


FIG. 5: Linear (dashed, \mathcal{R}^{MS}) and reconstructed (solid, \mathcal{R}^{NR}) binned dimensionless spectra ($\Delta[\cdot] = \frac{k^3}{2\pi^2} |\cdot|^2$) in the inflection inflation case from initial (navy blue) to final (red) times. Contours account for the full range of points in each bin. Fourier bins are those of the lattice with more than 10 realisations. $M_{\text{Pl}} = 100$.

an ultra-slow roll model. Reserving a more thorough investigation for future work, including different types of inflationary histories, we simply report here on the validation and potential of our stochastic method. The two scenarios studied are presented in Table I together with their extracted background evolution for the relevant e-fold span in Figure 1.

Figures 2 and 3 report the evolution of a simple quadratic inflation scenario and thus slow-roll (SR) dynamics. Modes enter the simulation for about 3.5 – 4 e-folds as can be seen for the growth of the contrasts in Figure 2. Afterwards quantities such as \mathcal{R} freeze as expected in the super-Hubble regime. The dynamics of such vanilla scenario are well-known and a good test that linear physics is recovered. This is particularly visible in the comparison of the spectrum extracted from the NR simulation \mathcal{R}^{NR} and the Mukhanov-Sasaki solution \mathcal{R}^{MS} in Figure 3, once the window has fully rolled from the IR to the UV. Note that the extraction of \mathcal{R}^{NR} from the evolved BSSN variables was detailed in Appendix B of [29] and involves i) subtraction of the box background, ii) reconstruction of Φ from BSSN conformal factor and metric, and iii) linear combination $\mathcal{R}^{\text{NR}} = \Phi - \langle K \rangle (\phi - \langle \phi \rangle) / 3 \langle \Pi \rangle$ in this gauge.

An ultra slow-roll phase (USR), $\varepsilon_1 \sim 0$ and $\varepsilon_2 \sim 6$ in our notations, is famously known for enhancing the power spectrum of modes after crossing the horizon [47]. In general, slow-roll-breaking regimes can be reached using features of various forms in the inflatonic potential, see,

for instance, [48]. Our potential is motivated by Higgs inflation [34, 35] and has been slightly tuned to show interesting physics within a few e-folds.

In this work, the lattice contains modes entering the IR system during the USR phase as well as during the transition from SR to USR, a numerically challenging regime because of the extreme slow-down of the field and the importance of the gradients. This has been at the heart of issues and fixing attempts in gradient-agnostic literature using the separate universe approximation and thus for δN formalisms [49] or standard stochastic inflation [27, 28]. Our simulations are run with $\sigma = 1$ and are fully gradient-enabled, which is unprecedented in a stochastic framework, whether it is for USR or not.

Real space inhomogeneities are displayed in Figure 4, where we report the contrasts of key quantities. The top three panels, show the progressive entry of all modes with their full amplitude within about 4 e-folds. The final part of the transition from SR to USR triggers a squeezing of the contrast for the field and the extrinsic curvature. USR then takes over for 2 to 3 e-folds and then starts a transition out of the inflection. In this phase, a lot of the modes making up \mathcal{R}^{NR} are already superHubble and undergo enhancement, later joined by the last ones to cross, as can be seen in the gauge-invariant extraction shown in the fourth panel. The contrast reached in this phase before the freezing of the modes reaches the non-perturbative value of 10 for the furthest outliers in real space.

Up to a certain maximum inhomogeneity amplitude (usually defined for dimensionless power spectrum as $\Delta[\mathcal{R}] \sim 1$ [50]), and due to the $\varepsilon_1 \rightarrow 0$ limit, USR is usually assumed to be well-described by the linear solution from the Mukhanov-Sasaki equation, despite reaching non-perturbative amplitudes. This is visible for the spectra displayed in Figure 5, which, at complete overlap of the closed linear and open IR non-linear system, shows excellent agreement.⁶ We note that, despite reaching up to $\Delta[\mathcal{R}] \sim 0.1 - 1$, no significant departure from the linear prediction is observed unlike [51]. In the future, a fully quantitative study will make detailed comparisons in this limit.

We note the last two panels of Figures 2 and 4 as a crucial verification of both our numerical and theoretical pipeline. In fact, we claimed satisfaction of the constraints at first order in the noise. To evaluate the order of the terms in the constraints, we define the *absolute constraint magnitudes* $[\mathcal{H}]$ and $[\mathcal{M}]$, calculated by summing the absolute value of the individual terms in the constraints.⁷ In its entry phase, the noise in \mathcal{R} has a maximum amplitude of $\sim 10^{-5}$. In both scenarios, the Hamiltonian constraint shows violation at the next order in perturbation theory ($\sim 10^{-10}$) when compared to the absolute magnitude $[\mathcal{H}]$. After that, inflation naturally damps the constraint.

For the Momentum constraint, being null at 0th order, the absolute magnitude $[\mathcal{M}]$ is the first order and we thus observe a second order violation as well in this phase. As a consistency check and similarly to [29], we find that switching any sign in our noise contributions yields a violation at first order (meaning $\mathcal{H}/[\mathcal{H}] \sim 10^{-5}$ and $\mathcal{M}/[\mathcal{M}] \sim 1$). In the quadratic case, the last mode crossing makes the $|\mathcal{M}|/[\mathcal{M}]$ momentarily a bit higher than second order because of the gradient resolution, which is acceptable given that a smaller k_{max} would fix that. A similar conclusion can be reached for the inflection case where $|\mathcal{M}|/[\mathcal{M}]$ sits later around 10^{-2} , which is acceptable given inhomogeneity of order 10 in \mathcal{R} at that point. This completes the validation and physicality check of our method, making it ready for future work on both fully non-perturbative and non-linear experiments for which no analytical results are known.

As a first demonstration of our method's potential, Appendix E analyses the evolution of the anisotropic degrees of freedom encoded in \tilde{K}_{ij} . In future work, applying the transverse projector will yield the first extraction of scalar-induced gravitational wave power from a Bunch-Davies vacuum evolved in NR. We reserve these investigations of PGWs for future work and focus on the general anisotropic amplitude in our two scenarios.

IV. CONCLUSION

In this work, we pioneered the full evolution of the Bunch-Davies vacuum in inflation using numerical relativity and the stochastic formalism. In the latter, modes do not all enter the simulation at the same initial time as done in our previous work [29] (see also [30] for tensor modes) but at a given elapsed time relative to their Hubble horizon crossing, thus better accounting for quantum diffusion. By achieving this, we provide a framework generalising stochastic inflation, inflationary numerical relativity and lattice cosmology beyond their standard assumptions.

Two test scenarios were studied, a very perturbative and linear case of slow-roll inflation and a potential with an inflection point triggering ultra slow-roll and so non-perturbative growth. All evolutions are successful, match expectations, and satisfy the constraints for our scales of interest, which is a substantial achievement for a stochastic framework and a strong validation that our pipeline is numerically and theoretically accurate. Moreover, we have removed the dependence of stochastic inflation on the separate universe approximation and its numerous caveats.

The possibilities offered by this new method are numerous and will shed light on new inflationary physics. For instance, we hope to provide specific studies, to gain more accurate insights on models such as ultra slow-roll and primordial black hole production, which have been at the centre of attention but also debates in the past years because of the aforementioned approximations. By including full General Relativity, we are now able to confront previous work as well as giving new signals such as fully non-linear primordial gravitational waves, including scalar-induced ones. For all fields evolved in their semi-classical portion of spacetime, we will also be able to extract non-Gaussianities of a new kind, whether they are additional scalars or from the tensorial sector. Finally, special attention will be given to regimes where quantum-diffusion dominates, where stochasticity is key. Therefore, upcoming experiments can look forward to an enlarged testable inflationary landscape.

ACKNOWLEDGMENTS

For their advice, expertise and excellent work on developing core software for the GRTL collaboration, thanks go to J. Kwan and M. Radia, supported by the Intel oneAPI COE and STFC DiRAC. Thanks are also to be given by Y.L. to other colleagues for insightful and supportive conversations, notably E. Florio, C. McCulloch, E. Pajer, S. Renaux-Petel, R. Bond, and E. Tomberg. Y.L. is supported by the STFC DiS-CDT scheme and the Kavli Institute for Cosmology, Cambridge. E.P.S.S. acknowledges funding from STFC Consolidated Grant No. ST/P000673/1. Computational resources were supported by STFC DiRAC HPC Facility (www.dirac.ac.uk)

⁶ This can also be confirmed by extracting the non-linear generalisation of \mathcal{R} , introduced in [29], showing no difference.

⁷ See eq. (32) in [29] for the exact definition.

funded by BEIS capital funding via STFC Capital Grants ST/P002307/1 and ST/R002452/1 and STFC Operations Grant ST/R00689X/1 and a grant from G-research. Y.L. thanks the CoBaL and Inflation 2025 conference committees and sponsors for their financial support.

REFERENCES

- [1] Y. L. Launay, G. I. Rigopoulos, and E. P. S. Shellard, *Phys. Rev. D* **109**, 123523 (2024).
- [2] Planck Collaboration, Y. Akrami, and et al., *Astronomy & Astrophysics* **641**, A9 (2020), [arXiv:1905.05697](#).
- [3] E. Chaussidon and et al., *Journal of Cosmology and Astroparticle Physics* **2025**, 029 (2025).
- [4] A. Chudaykin, M. M. Ivanov, and O. H. E. Philcox, (2025), [arXiv:2512.04266](#).
- [5] R. M. Wald, *Quantum Field Theory in Curved Space-Time and Black Hole Thermodynamics*, Chicago Lectures in Physics (University of Chicago Press, Chicago, IL, 1995).
- [6] J. Maldacena, *Journal of High Energy Physics* **2003**, 013 (2003).
- [7] D. J. Mulryne and J. W. Ronayne, *J. Open Source Softw.* **3**, 494 (2018).
- [8] D. Werth, L. Pinol, and S. Renaux-Petel, “Cosmological Flow of Primordial Correlators,” (2023).
- [9] A. Costantini, L. Iacconi, and D. J. Mulryne, *JCAP* **09**, 077 (2025), [arXiv:2503.15194](#).
- [10] A. A. Starobinsky, in *Field Theory, Quantum Gravity and Strings*, Vol. 246, edited by H. J. De Vega and N. Sánchez (Springer Berlin Heidelberg) pp. 107–126.
- [11] M. Morikawa, *Physical Review D* **42**, 1027.
- [12] D. S. Salopek and J. R. Bond, *Physical Review D* **43**, 1005 (1991).
- [13] D. Wands, K. A. Malik, D. H. Lyth, and A. R. Liddle, *Physical Review D* **62**, 043527.
- [14] V. Vennin and A. A. Starobinsky, *The European Physical Journal C* **75** (2015).
- [15] K. Clough, *Scalar Fields in Numerical General Relativity: Inhomogeneous inflation and asymmetric bubble collapse*, Ph.D. thesis, King’s Coll. London, Cham (2017).
- [16] G. Felder and I. Tkachev, *Computer Physics Communications* **178**, 929 (2008).
- [17] A. Caravano, “Simulating the inflationary universe: from single-field to the axion-u(1) model,” (2022).
- [18] F. Finelli, G. Marozzi, A. A. Starobinsky, G. P. Vacca, and G. Venturi, *Physical Review D* **79**, 044007 (2009).
- [19] F. Finelli, G. Marozzi, A. A. Starobinsky, G. P. Vacca, and G. Venturi, *Physical Review D* **82**, 064020 (2010).
- [20] C. Pattison, V. Vennin, H. Assadullahi, and D. Wands, *Journal of Cosmology and Astroparticle Physics* **2019**, 031 (2019).
- [21] J. H. Jackson, H. Assadullahi, K. Koyama, V. Vennin, and D. Wands, *Journal of Cosmology and Astroparticle Physics* **2022**, 067 (2022).
- [22] D. G. Figueroa, S. Raatikainen, S. Rasanen, and E. Tomberg, *Physical Review Letters* **127**, 101302.
- [23] D. G. Figueroa, S. Raatikainen, S. Räsänen, and E. Tomberg, *Journal of Cosmology and Astroparticle Physics* **2022**, 027 (2022).
- [24] E. Tomberg, *Journal of Cosmology and Astroparticle Physics* **2023**, 042 (2023).
- [25] Y. Mizuguchi, T. Murata, and Y. Tada, *Journal of Cosmology and Astroparticle Physics* **2024**, 050 (2024).
- [26] D. Artigas, J. Grain, and V. Vennin, *Journal of Cosmology and Astroparticle Physics* **2022**, 001.
- [27] J. H. P. Jackson, H. Assadullahi, A. D. Gow, K. Koyama, V. Vennin, and D. Wands, (2023), [arXiv:2311.03281](#).
- [28] V. Briaud, R. Kawaguchi, and V. Vennin, (2025), [arXiv:2509.05124](#).
- [29] Y. L. Launay, G. I. Rigopoulos, and E. P. S. Shellard, *Phys. Rev. D* **112**, 043518 (2025), [arXiv:2502.06783](#).
- [30] E. Florio and E. P. S. Shellard, (2024), [arXiv:2412.19731](#).
- [31] Y. L. Launay, G. I. Rigopoulos, and E. S. Shellard, *Journal of Cosmology and Astroparticle Physics* **2025**, 071 (2025).
- [32] L. P. Levasseur and E. McDonough, *Physical Review D* **91**, 063513.
- [33] E. Tomberg, (2024), [arXiv:2411.12465](#).
- [34] Y. Hamada, H. Kawai, K.-y. Oda, and S. C. Park, *Phys. Rev. Lett.* **112**, 241301 (2014), [arXiv:1403.5043](#).
- [35] F. Bezrukov and M. Shaposhnikov, *Physics Letters B* **734**, 249 (2014).
- [36] T. W. Baumgarte and S. L. Shapiro, *Physical Review D* **59**, 024007 (1998).
- [37] M. Shibata and T. Nakamura, *Physical Review D* **52**, 5428 (1995).
- [38] GRTL collaboration, “GRTEclyn,” (2024).
- [39] K. Clough, P. Figueras, H. Finkel, M. Kunesch, E. A. Lim, and S. Tunyasuvunakool, *Classical and Quantum Gravity* **32**, 245011 (2015).
- [40] T. Andrade and et al., *Journal of Open Source Software* **6**, 3703 (2021).
- [41] W. Zhang and et al., *Journal of Open Source Software* **4**, 1370 (2019).
- [42] D. Alic, C. Bona-Casas, C. Bona, L. Rezzolla, and C. Palenzuela, *Physical Review D* **85** (2012), [10.1103/physrevd.85.064040](#).
- [43] D. Alic, W. Kastaun, and L. Rezzolla, *Physical Review D* **88** (2013), [10.1103/physrevd.88.064049](#).
- [44] J. C. Aurrekoetxea, K. Clough, and E. A. Lim, “Cosmology using numerical relativity,” (2024), [arXiv:2409.01939](#).
- [45] F. J. Agocs, W. J. Handley, A. N. Lasenby, and M. P. Hobson, *Phys. Rev. Res.* **2**, 013030 (2020).
- [46] S. Winitzki and A. Vilenkin, *Phys. Rev. D* **61**, 084008 (2000).
- [47] S. M. Leach, M. Sasaki, D. Wands, and A. R. Liddle, *Phys. Rev. D* **64**, 023512 (2001), [arXiv:astro-ph/0101406](#).
- [48] S. S. Mishra and V. Sahni, *JCAP* **04**, 007 (2020), [arXiv:1911.00057](#).
- [49] D. Artigas, S. Pi, and T. Tanaka, *Phys. Rev. Lett.* **134**, 221001 (2025), [arXiv:2408.09964](#).
- [50] G. Franciolini, A. J. Iovino, M. Taoso, and A. Urbano, *Phys. Rev. D* **109**, 123550 (2024).
- [51] A. Caravano, G. Franciolini, and S. Renaux-Petel, (2024), [arXiv:2410.23942](#).
- [52] K. Burrage, P. Burrage, D. J. Higham, P. E. Kloeden, and E. Platen, *Phys. Rev. E* **74**, 068701 (2006).
- [53] A. Rössler, *SIAM J. Numer. Anal.* **48**, 922 (2010).
- [54] D. Cruces and C. Germani, *Physical Review D* **105**, 023533.
- [55] D. S. Salopek and J. R. Bond, *Physical Review D* **42**, 3936 (1990).
- [56] G. I. Rigopoulos and E. P. S. Shellard, *Physical Review D* **68**, 123518 (2003).

- [57] T. Prokopec and G. Rigopoulos, *Physical Review D* **104**, 083505 (2021).
 [58] D. Artigas, E. Frion, T. Miranda, V. Vennin, and D. Wands, *JCAP* **08**, 032 (2025), arXiv:2504.05937.

Appendix A: Gauge invariants as functionals of \mathcal{R}

The scalar linear constraints of general relativity write

$$\left\{ \begin{array}{l} 4\Delta\Phi - 4H\kappa - 2M_{\text{Pl}}^{-2}\delta\rho = 0, \\ -2\partial_i \left[\Delta\chi + \kappa - \frac{3}{2}M_{\text{Pl}}^{-2}\frac{\dot{\phi}_b}{\alpha_b}\delta\phi \right] = 0, \end{array} \right. \quad (\text{A1})$$

where $\chi \equiv -\frac{a^2}{\alpha_b}(B - \dot{E})$, $\kappa \equiv 3\left(\frac{\dot{\phi}}{\alpha_b} + H\Psi\right) - \Delta\chi$, and $\delta\rho = \frac{\dot{\phi}_b}{\alpha_b}\frac{\delta\dot{\phi}}{\alpha_b} + \frac{dV}{d\phi}(\phi_b)\delta\phi - \frac{\dot{\phi}_b^2}{\alpha_b^2}\Psi$.

In the following we set $\alpha_b = 1$, working in cosmic background time w.l.o.g. We can chose for convenience the comoving gauge where $\delta\phi^{co} = E^{co} = 0$, and one has

$$\left\{ \begin{array}{l} \delta\rho^{co} = -\dot{\phi}_b^2\Psi^{co}, \\ \chi^{co} = -a^2B^{co}, \\ \kappa^{co} = 3(\dot{\Phi}^{co} + H\Psi^{co}) + a^2\Delta B^{co}, \end{array} \right. \quad (\text{A2})$$

together with $\mathcal{R}^{co} = \Phi^{co}$. Equation (A1) thus reduces to

$$\left\{ \begin{array}{l} \Delta\mathcal{R}^{co} - a^2H\Delta B^{co} = -\frac{1}{2}M_{\text{Pl}}^{-2}\dot{\phi}_b^2\Psi^{co}, \\ \dot{\mathcal{R}}^{co} + H\Psi^{co} = 0, \end{array} \right. \quad (\text{A3})$$

which is straightforward to solve in Fourier space

$$\left\{ \begin{array}{l} B^{co} = a^{-2}H^{-1}\mathcal{R}_k^{co} + \varepsilon_1 k^{-2}\dot{\mathcal{R}}_k^{co}, \\ \Psi^{co} = -H^{-1}\dot{\mathcal{R}}_k^{co}. \end{array} \right. \quad (\text{A4})$$

Together with χ^{co} and $\delta\rho^{co}$, all quantities needed to evaluate the linear gauge invariant variables of eq. (2) are known, yielding eq. (3) in the comoving gauge. These are relations between gauge invariant variables and are therefore also true for any other gauge choice.

Appendix B: BSSN equations

The BSSN reformulation of the ADM equations reads

$$\left\{ \begin{array}{l} \partial_t X - \frac{2}{3}X\alpha K + \frac{2}{3}X\partial_k\beta^k - \beta^k\partial_k X = \mathcal{F}^{-1}\{\mathcal{S}_X^{BSSN}\}, \\ \partial_t\tilde{\gamma}_{ij} + 2\alpha A_{ij} - \tilde{\gamma}_{ik}\partial_j\beta^k - \tilde{\gamma}_{jk}\partial_i\beta^k \\ + \frac{2}{3}\tilde{\gamma}_{ij}\partial_k\beta^k - \beta^k\partial_k\tilde{\gamma}_{ij} = \mathcal{F}^{-1}\{\mathcal{S}_{\tilde{\gamma}_{ij}}^{BSSN}\}, \\ \partial_t K + \gamma^{ij}D_i D_j \alpha - \alpha \left(A_{ij}A^{ij} + \frac{1}{3}K^2 \right) \\ - \beta^i\partial_i K - 4\pi\alpha(\rho + S) = \mathcal{F}^{-1}\{\mathcal{S}_K^{BSSN}\}, \\ \partial_t A_{ij} - X \left[-D_i D_j \alpha + \alpha (R_{ij} - M_{\text{Pl}}^{-2}\alpha S_{ij}) \right]^{TF} \\ - \alpha (K A_{ij} - 2A_{il}A_{jl}) - A_{ik}\partial_j\beta^k - A_{jk}\partial_i\beta^k \\ + \frac{2}{3}A_{ij}\partial_k\beta^k - \beta^k\partial_k A_{ij} = \mathcal{F}^{-1}\{\mathcal{S}_{A_{ij}}^{BSSN}\}, \\ \partial_t\tilde{\Gamma}^i - 2\alpha \left(\tilde{\Gamma}_{jk}^i A^{jk} - \frac{2}{3}\tilde{\gamma}^{ij}\partial_j K - \frac{3}{2}A^{ij}\frac{\partial_j X}{X} \right) \\ + 2A^{ij}\partial_j\alpha - \beta^k\partial_k\tilde{\Gamma}^i - \tilde{\gamma}^{jk}\partial_j\partial_k\beta^i - \frac{1}{3}\tilde{\gamma}^{ij}\partial_j\partial_k\beta^k \\ - \frac{2}{3}\tilde{\Gamma}^i\partial_k\beta^k + \tilde{\Gamma}^k\partial_k\beta^i + 2M_{\text{Pl}}^{-2}\alpha\tilde{\gamma}^{ij}S_j = \mathcal{F}^{-1}\{\mathcal{S}_{\tilde{\Gamma}}^{BSSN}\}, \\ \partial_t\phi - \alpha\Pi - \beta^i\partial_i\phi = 0, \\ \partial_t\Pi - \beta^i\partial_i\Pi - \alpha\partial_i\partial^i\phi - \partial_i\phi\partial^i\alpha \\ - \alpha \left(K\Pi - \gamma^{ij}\tilde{\Gamma}_{ij}^k\partial_k\phi - \frac{dV}{d\phi} \right) = \mathcal{F}^{-1}\{\mathcal{S}_{\Pi}^{BSSN}\}, \\ \mathcal{H} = R + K^2 - K_{ij}K^{ij} - 2M_{\text{Pl}}^{-2}\rho = \mathcal{F}^{-1}\{\mathcal{S}_{\mathcal{H}}^{BSSN}\}, \\ \mathcal{M}_i = D^j(\gamma_{ij}K - K_{ij}) - M_{\text{Pl}}^{-2}S_i = \mathcal{F}^{-1}\{\mathcal{S}_{\mathcal{M}}^{BSSN}\}, \end{array} \right. \quad (\text{B1})$$

where the metric is written as in eq. (19) up to a minus sign convention for the shift β^i and where we have introduced the conformal metric and factor, the conformal traceless extrinsic curvature and the contraction of the conformal metric connection

$$\left\{ \begin{array}{l} \gamma_{ij} = \frac{1}{X}\tilde{\gamma}_{ij}, \\ X = (\det\gamma_{ij})^{-\frac{1}{3}}, \\ A_{ij} = X\tilde{K}_{ij}, \\ \tilde{\Gamma}^i = \tilde{\gamma}^{jk}\tilde{\Gamma}_{jk}^i, \end{array} \right. \quad (\text{B2})$$

and where the r.h.s. Fourier transforms were computed in [1] as

$$\left\{ \begin{array}{l} \mathcal{S}_K^{BSSN} = -\varepsilon_1\mathcal{S}_{\mathcal{R}}, \\ \mathcal{S}_{A_{ij}}^{BSSN} = \varepsilon_1\left(\frac{1}{3}\delta_{ij} - k^{-2}k_ik_j\right)\mathcal{S}_{\mathcal{R}}, \\ \mathcal{S}_{\Pi}^{BSSN} = \sqrt{2\varepsilon_1}M_{\text{Pl}}\mathcal{S}_{\mathcal{R}}, \end{array} \right. \quad (\text{B3})$$

and all others being perfectly vanishing.

Note that this work does not implement the tensor sources, derived in [1].

Appendix C: Numerical and stochastic schemes

At each time step and for the vector of fields \mathcal{X} , such that $\partial_t \mathcal{X} = \mathcal{G}[\mathcal{X}(t), t, \mathbf{x}] = \text{BSSN}[\mathcal{X}(t), t, \mathbf{x}] + \mathcal{I}[t, \mathbf{x}]$, then the 4th order Runge-Kutta (RK4) scheme writes

$$\mathcal{X}(t + \Delta t, \mathbf{x}) = \mathcal{X}(t, \mathbf{x}) + \left(\frac{1}{6}\mathcal{K}_1 + \frac{1}{3}\mathcal{K}_2 + \frac{1}{3}\mathcal{K}_3 + \frac{1}{6}\mathcal{K}_4 \right) \Delta t,$$

where each term writes sequentially as

$$\begin{cases} \mathcal{K}_1 = \mathcal{G}[\mathcal{X}(t), t, \mathbf{x}], \\ \mathcal{K}_2 = \mathcal{G}[\mathcal{X}(t) + \mathcal{K}_1 \frac{\Delta t}{2}, t + \frac{\Delta t}{2}, \mathbf{x}], \\ \mathcal{K}_3 = \mathcal{G}[\mathcal{X}(t) + \mathcal{K}_2 \frac{\Delta t}{2}, t + \frac{\Delta t}{2}, \mathbf{x}], \\ \mathcal{K}_4 = \mathcal{G}[\mathcal{X}(t) + \mathcal{K}_3 \Delta t, t + \Delta t, \mathbf{x}]. \end{cases} \quad (\text{C1})$$

The subtlety here is the stochastic contribution of the r.h.s. $\mathcal{I}[t, \mathbf{x}] = \mathcal{F}^{-1}\{\mathcal{S}_k(t)\alpha_{\mathbf{k}}\}$ writing generically $\mathcal{S}_k(t) = a_k^{\mathcal{X}}(t)\ddot{W}_k(t) + b_k^{\mathcal{X}}(t)\dot{W}_k(t)$. Note that with stochastic backreaction, \mathcal{I} becomes a function of the fields as well. In stochastic PDE language, applying the RK4 method to the stochastic contribution does not give the same convergence for the stochastic part [52], rather that of the Euler–Maruyama method. In the future, we could use a proper stochastic scheme such as those given in [53] and used in [54]. However, this would take significant edits in the AMREX core and we expect very little impact if the sources are kept in the perturbative regime compared to the background.

Appendix D: Design of the space to time ratio

Let Δt be the time step, N_T the number of time steps, and $\theta = \Delta t/dx$ the Courant factor, which has an upper bound for stability. We are interested in probing the crossing of all modes in our lattice, from k_{min} to $k_{max}^{\mathcal{R}}$. Let us assume that our simulation's expansion is roughly that of a De Sitter universe with a constant H^{\otimes} , so that $k_{\sigma}(t) \simeq \sigma H^{\otimes} e^{\mathcal{N}}$, where $\mathcal{N} = H^{\otimes}(t - t^{\otimes})$ is the number of e-folds since the start of the simulation. This provides a proxy to compute the number of e-folds between the first and the last mode crossing

$$\mathcal{N}^{\otimes} = \ln \left(\frac{k_{max}^{\mathcal{R}}}{k_{min}} \right) = \ln \left(\frac{N}{n} \right).$$

Our simulation needs to last up to that time, together with an amount $\Delta \mathcal{N}$ of supplementary e-folds for the study of the superHubble regime. The feasibility of this study thus depends entirely on our computational resources with respect to the value of N .

The choice of the time-to-space ratio θ is the most constrained one. Beyond the Courant upper bound and stability in general, the choice of θ is still key. Given the

physical duration $\mathcal{N}_{tot} = \mathcal{N}^{\otimes} + \Delta \mathcal{N}$, the number of time steps is

$$N_T \simeq \frac{\mathcal{N}_{tot}}{H^{\otimes} \Delta t} = \frac{N\sigma}{2\pi\theta} (\mathcal{N}^{\otimes} + \Delta \mathcal{N}).$$

In other words, trying to reach an excessively small value for θ will jeopardize our chances to run the simulation in a reasonable time.

Instinctively, the choice of θ also controls the number of modes entering the simulation per time step. Indeed, when approximating the shift in the window's range between t and $t + \Delta t$ as $\Delta k_{\sigma}(t) \simeq k_{\sigma}(t) H \Delta t$, we infer that the ratio to the gap before the next discrete mode is

$$\frac{\Delta k_{\sigma}(t)}{k_{min}} \simeq \frac{2\pi\theta}{N\sigma} e^{\mathcal{N}(t)},$$

which essentially says that the window has an exponentially growing range. For a given \mathcal{N}^{\otimes} and σ , one can in particular pick θ such that no more than one discrete mode enters the lattice per time step, by requiring $\Delta k_{\sigma}^{\otimes} \leq k_{min}$, or equivalently

$$\theta < \frac{n\sigma}{2\pi},$$

which is more constraining than the stability condition only on superHubble cutoffs ($\sigma < 1$).

It is important to note that for $\sigma \geq 1$, the simulation will not see more than one discrete mode enter at a time if sticking to the Heaviside windowing or a sharp enough window. Using a smooth window function prevents stochastic spikes from happening in that sense.

Appendix E: A first look at anisotropic DOFs

Discarding the anisotropic degrees of freedom of General Relativity is central to the separate universe approximation (SUA) [13] and the Hamilton-Jacobi approach [55–57]. With a fully relativistic evolution of Bunch-Davies fluctuations, we can confirm if this is appropriate and understand the validity of such approximations more quantitatively. We know of course that K 's background ($k = 0$ mode) is dominating overall given that \tilde{K} has no background order contribution. We are interested in the perturbations at first and second order in perturbation theory, in particular in the case of USR where \mathcal{R} blows up. For that purpose Figure 6 shows the spectra of K , \tilde{K} (taken as $\tilde{K}_{ij}(k)\tilde{K}^{ij}(k)^*$ in Fourier space) and $\sqrt{3\tilde{K}_{ij}\tilde{K}^{ij}/2}$.

It is of interest to compare the anisotropic ($-\tilde{K}_{ij}\tilde{K}^{ij}$) and isotropic ($\frac{2}{3}K^2$) contributions to the Hamiltonian constraint, given that the latter is the only one commonly considered in the SUA. Note that K and \tilde{K} (not squared) do not compete in any of the ADM equations without being squared or contracted respectively, see eqns. (16)

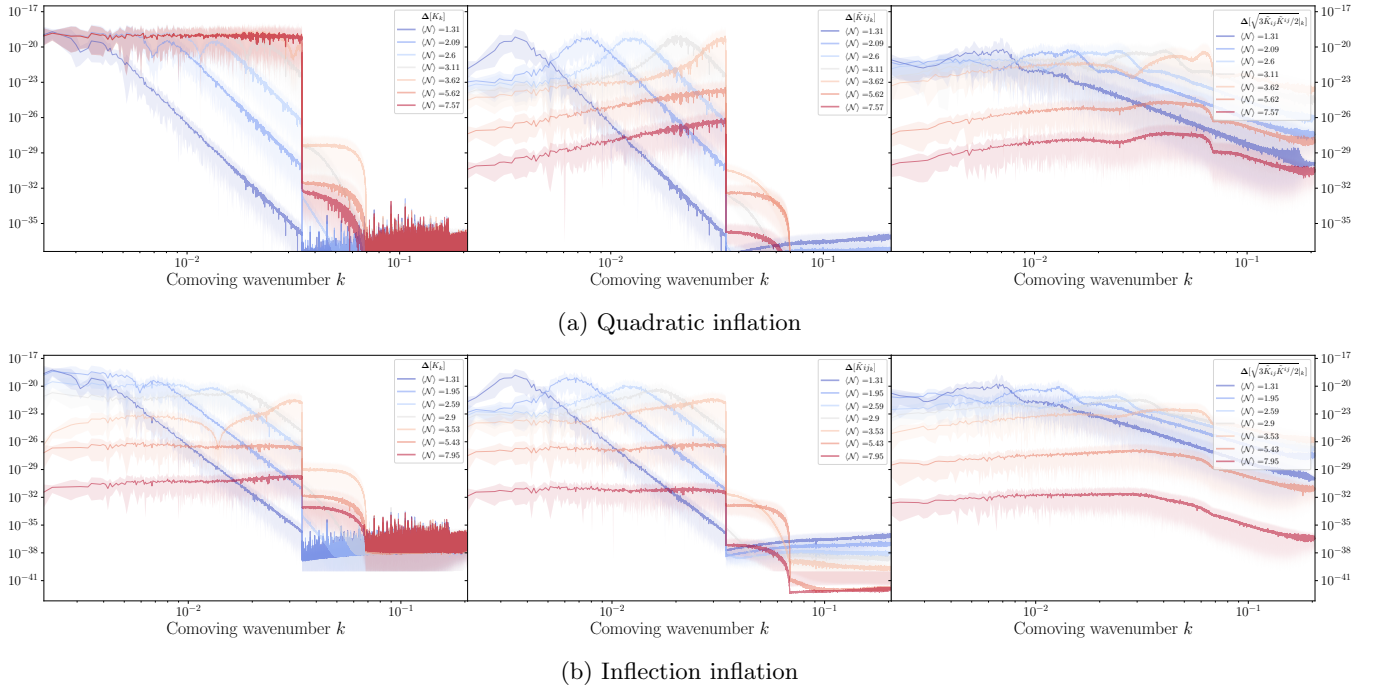


FIG. 6: Binned dimensionless spectra ($\Delta[\cdot] = \frac{k^3}{2\pi^2} |\cdot|_k^2$) of K , \tilde{K} , and $\sqrt{3\tilde{K}_{ij}\tilde{K}^{ij}/2}$ in the quadratic (top) and inflection inflation case (bottom) from initial (navy blue) to final (red) times. Contours account for the full range of points in each bin. Fourier bins are those of the lattice with more than 10 realisations. $M_{\text{Pl}} = 100$.

- (20) - (21) and (24), apart from the Momentum constraint (25), usually identified as the culprit hampering such approximation [54, 58].

Looking at the left panels first, we find that perturbations in K freeze in the quadratic slow-roll case but decay in the USR case. This is also visible in the contrasts present in Figures 2 and 4. Switching to the second panels, we see that anisotropic and isotropic powers can be comparable in magnitude in both scenarios initially but the former decays quickly after horizon crossing and are thus negligible in the quadratic case. In the USR case, perturbations in K decay as well, implying that all terms in K_{ij} are of similar magnitude and that the SUA

truncation of the momentum constraint could potentially be violated.

The last panel probes most relevant terms competing with \tilde{K} : these are expected to be of second order given that \tilde{K} has no background order, and, in fact, a careful observation shows anisotropic spectra to be subdominant to the isotropic modes for most times. As pointed out in [58] through the concept of non-adiabatic pressure, the anisotropic sector cannot be neglected a priori for the satisfaction of the momentum constraint in regimes such as this one. Further quantitative comparison between the isotropic and anisotropic parts of the extrinsic curvature is left for future work.